International Journal of
Georesources and Environment
http://ijge.camdemia.ca, ijge@camdemia.ca
IJGE 2018 4(3): 105-114
Available at http://ojs.library.dal.ca/ijge
Research and Development and Industry

Development of a Laboratory for Testing the Accuracy of Terrestrial 3D Laser Scanning Technologies

Frederick Cawood[1*], Mei Yu[2], Peter Kolapo[1], Changbiao Qin[1]
[1] Wits Mining Institute, University of the Witwatersrand, Johannesburg, South Africa
[2] School of Environmental and Spatial Informatics, China University of Mining and Technology, Xuzhou, China

Abstract: The mining market is currently overwhelmed by technology vendors offering scanning equipment as 'solutions' for real time mapping and monitoring rock mass movement for mine safety. Mines are left with a problem in that the technology is mostly unproven and not originally designed for mine safety accuracies. Scanning system accuracy assessment needs to be done so as to increase the level of confidence and trust in the quality of the results. The scope of this research is set a laboratory for testing terrestrial laser scanning (TLS) systems – complete with targets fix on the wall of the testing laboratory, which plays a vital role in creating high quality and reliable digital point clouds. To improve the accuracy test of the scanning system, we support exact positioning and distance measurement of points cloud by providing revolutionizing surveying solutions and infrastructure development. The FARO, a static 3D laser scanner and uGPS, a mobile 3D laser scanning system are tested in this research. If the level of accuracy of these TLS systems can be ascertained, this can fit into the production process, ore flow analysis to measure discrepancy and metal accounting principles. Notably, this will add value to mining operations chains through measurement and adequate monitoring of process by revealing the modifying factor contributing to mine loss. More importantly good decisions can be made on mine evacuation when point cloud comparisons raise alarm on rock mass movement. With this laboratory, we can offer a vital service to the mining industry by certifying new scanning solutions as these arrive on the market. This will make mines safer.

Keywords: mine safety, TLS, accuracy evaluation, FARO, mobile 3D laser scanning system

1 Introduction

The aim of this study is to test the point clouds generated by scanning systems for both precision and accuracy. Both criteria are important when applying scanning data to mining problems such as surveying, mapping and monitoring surfaces for rock engineering use. The need for this study was raised by Gold Fields' South Deep mine, which is an underground South African mine who bought such a system to establish rock movement over time. The initial results obtained at South Deep were questionable and the Wits Mining Institute (WMI) was requested to do more testing in a laboratory set-up for this purpose. The work is significant because scanning systems have the potential to contribute to real-time positioning, mapping, navigation and monitoring rock movements in the underground mining environment. Scanning systems are therefore an enabler for good safety, health and economic decisions in mining. What's special about our approach is its fundamental nature to analyse point cloud data from both precision and accuracy perspectives. Such tests were conducted in a fit-for-purpose laboratory. The results certainly contribute to a better understanding of a fairly new topic in mining.

This article contains first, a literature review on the topic. This is followed by a description of the short-range laboratory, where after the establishment of accurate survey control inside the laboratory is explained. Sections five and six describe the scanners and the data analysis, followed by the conclusion and recommendation. The main findings were that first, scanning systems are very useful in mining and second, deep understanding of the fundamentals are required in order to achieve both accuracy and precision – especially when scanning from a moving platform.

2 Literature Review

2.1 3D laser scanning

3D Laser Scanning is a non-contact, non-destructive technology that digitally captures the shape of physical objects using a line of laser light. Because of the ability of fast, reliable and inexpensive 3D survey, it has become popularly used in variety applications such as change detection (Vaaja et al 2011, Lindenbergh and Pietrzyk 2015, Mukupa et al 2016) and deformation tracking (Mukupa et al 2016, Jafari et al 2017), cave and mine surveying (Zlot and Bosse 2014a, Zlot and Bosse 2014b, Grehl et al 2015) etc. The laser scanner is able to record millions of 3D points. These X, Y, Z measurements can be imported into specific CAD design software and displayed on a computer monitor

* Corresponding Author: Frederick Cawood, Email: Frederick.Cawood@wits.ac.za, phone: +27 11 717 7428
Copyright © 2018 Canamaple Academia Services, http://press.camdemia.ca
DOI: 10.15273/ijge.2018.03.018

as 'point clouds', which have photographic qualities portrayed in one-color, grayscale, false-colour or even true colour. The files with the point clouds can be viewed, navigated, measured and analysed as 3D models (Puente et al 2013).

2.2 Principle of laser scanning

In current laser scanning systems, two techniques are mainly used for range measurements time-of-flight (TOF) and phase shift. TOF scanner sends a short laser pulse to the target, and the time difference between the emitted and received pulses is used to determine the range. The range r is calculated the following equation:

$$r = \frac{1}{2} c\Delta t \tag{1}$$

where c is the speed of light and Δt is the time of flight of the pulse.

In contrast, phase-based laser scanners use the phase difference between the emitted and received backscattered signal of an amplitude modulated continuous wave (AM CW) to determine the range. Phase shift laser scanners are more accurate, but their measurement range is shorter. The relationship between the phase shift and range is provided by the following equation:

$$r = \frac{\Delta\varphi}{2\pi}\frac{\lambda}{2} + \frac{\lambda}{2}n \tag{2}$$

where λ is the modulation wavelength, φ is the phase shift and n is the unknown number of full wavelengths between the sensor system and the reflecting object.

The coordinate of target in scanner coordinate system (in Figure 1) is calculated according to the range r, horizontal scanning angle α and vertical scanning angle θ following (3). α And θ are measured by high-precision engineered encoders.

$$\left.\begin{aligned} X &= r\cos\theta\cos\alpha \\ Y &= r\cos\theta\sin\alpha \\ Z &= r\sin\theta \end{aligned}\right\} \tag{3}$$

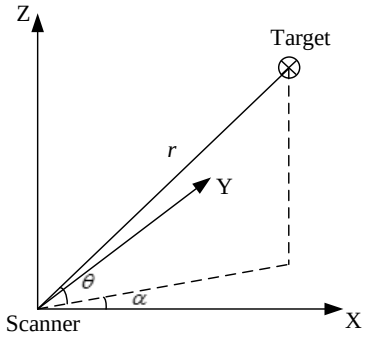

Figure 1 The coordinate of target in scanner coordinate system

2.3 Mobile laser scanning

Mobile laser scanning (MLS) is a ground-based laser scanning technology that obtain 3D points by using a laser scanner mounted on mobile system like vessel and land vehicle. It is more safety and efficiency compared with static laser scanning (Williams et al 2013).

MLS system generally consists of five subsystems: mobile platform, laser scanner, position system consisting of Global Navigation Satellite System (GNSS), Inertial Measurement Unit (IMU) inertial unit and Distance Measurement Indicators (DMIs), photogrammetric cameras or video cameras and on-board computer for controlling these components. Regarding the navigation technologies, the simultaneous localization and mapping (SLAM) is possibly used in MLS to decrease the cost of the IMU system required (Puente et al 2013).

2.4 Principle of MLS

The laser range of MLS is similar to static laser scanning containing TOF and phase shift two kinds. What's different is MLS use Global Navigation Satellite System (GNSS), Inertial Measurement Unit (IMU), Directional Movement Index (DMI) and simultaneous localization and mapping (SLAM) to determinate the time-variable position and orientation parameters for MLS system direct geo-referencing. Combining the laser range, scan angle obtained using high-precision engineered encoders, and laser position from position system, coordinates of the ground points for each laser pulse can be calculated (Puente et al 2013).

In MLS, there are three coordinate systems: the geo-spatial coordinate system (GCS-O), the POS body coordinate system (PCS-O) and the laser scanner coordinate system (LCS-O) (Mao et al 2015). The relationship between the three coordinate systems is displayed in Figure 2.

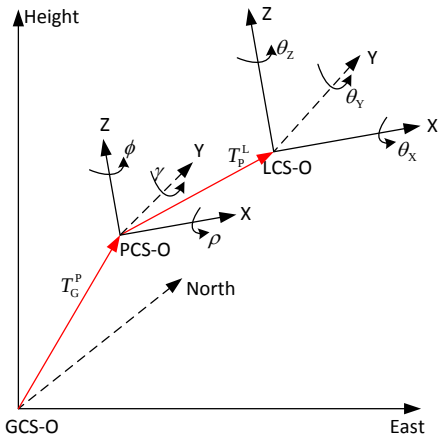

Figure 2 Relationship of geo-spatial coordinate system (GCS-O), POS body coordinate system (PCS-O) and laser scanner coordinate system (LCS-O)

The GCS-O is usually the Gauss coordinate system in which the X axis points to the east, the Y axis to the north and the Z axis up. The coordinates of LiDAR point clouds and control points fall under this coordinate system. The PCS-O is a right-handed system and is attached to the IMU: the origin is located in the IMU navigation centre, with the X axis pointing to the right, the Y axis pointing forward and

the Z axis pointing up. The LCS-O is also a right-handed system in which the X axis overlaps with the zero-degree laser beam, the Y axis is perpendicular to the X axis in the scanning plane and the Z axis is perpendicular to the scanning plane. The relationship between these coordinate systems is shown in Figure 2 (Mao et al 2015).

The raw data of the laser scanner were in the LCS-O and then transformed into the PCS-O with spatial alignment parameters, including three translations and three rotations, and, finally, transformed into the GCS-O with the position and orientation measured by the POS-O.

$$X_{\mathrm{G}} = T_{\mathrm{G}}^{\mathrm{P}} + R_{\mathrm{G}}^{\mathrm{P}}(R_{\mathrm{P}}^{\mathrm{L}} X_{\mathrm{L}} + T_{\mathrm{P}}^{\mathrm{L}}) \quad (4)$$

where the subscripts G, P , L indicate the GCS-O, PCS-O and LCS-O coordinate systems, respectively, X_{G} is the coordinate vector of the LiDAR point in the GCS-O, $T_{\mathrm{G}}^{\mathrm{P}} = [T_{\mathrm{E}} \quad T_{\mathrm{N}} \quad T_{\mathrm{H}}]^{\mathrm{T}}$ is the coordinate vector of the POS-O navigation centre in the GCS-O, $R_{\mathrm{G}}^{\mathrm{P}}$ is the rotation matrix from the PCS-O to GCS-O constituted from the orientation o ($o = [\gamma \quad \rho \quad \phi]^{\mathrm{T}}$, γ roll, ρ pitch, ϕ heading), X_{L} is the coordinate vector of the laser scanner measurement in the LCS-O, $T_{\mathrm{P}}^{\mathrm{L}} = [T_{\mathrm{X}} \quad T_{\mathrm{Y}} \quad T_{\mathrm{Z}}]^{\mathrm{T}}$ is the translation vector from the LCS-O to the PCS-O and $R_{\mathrm{p}}^{\mathrm{L}}$ is the rotation matrix constituted from the alignment angles ($\theta = [\theta_{\mathrm{X}} \quad \theta_{\mathrm{Y}} \quad \theta_{\mathrm{Z}}]^{\mathrm{T}}$).

The final MLS dataset represents millions of points with three-dimensional coordinates in the GCS-O.

2.5 Accuracy evaluation of MLS

In recent times, outstanding research has been conducted in order to establish the accuracy of MLS system. The accuracy assessment and control technologies can be classified as data driven or model driven. Data-driven technologies directly correct the point clouds using ground control points (GCPs). Model-driven technology analyses the error sources in the MLS and their impact on points and then proposes methods for the elimination and reduction of these errors (Mao et al 2015).

Barber et al (2008) assessed the precision and accuracy of data collected using the Street Mapper system. It shown the Street Mapper system is able to produce data with an RMS error in elevation of approximately 3 cm compared with RTK GPS and provide a measurement precision of similar order from the comparison of repeated data collection. This result demonstrated that systems can be successfully used in relatively built up areas.

Botes (2013) compared MLS with airborne laser scanning (ALS), photogrammetry and traditional ground surveying methods and shown MLS is capable of measuring at similar or better accuracies. They also assured that the quality of the product is well within the range of total station/GPS accuracies.

Kaartinen et al (2012) established a permanent urban test field to compare the point clouds generated by RIEGL, Optech and Street Mapper etc. Their experiment revealed that high-quality point clouds can be generated by all MLS systems under good GNSS conditions. With all professional systems properly calibrated, the elevation accuracy was better than 3.5 cm up to a range of 35 m. The best system had a planimetric accuracy of 2.5 cm even with range of 45 m.

Due to the difficulty of operating MLS without GNSS coverage, mapping a large-scale undergrounding mine in 3D is rarely accomplished. Zlot and Bosse used MLS for the first time to generate the 3D map of cave (Zlot and Bosse 2014a). They presented a laser-based SLAM solution to generate vehicle trajectory and 3D point cloud from data acquired while the vehicle continuously drives through an underground mine (Zlot and Bosse 2014b).

Permanent test field with accurate ground truth are valuable tools for analysing the performance of remote sensing systems and methods (Kaartinen et al 2012).

3 Laboratory Set up

3.1 Laboratory description

The scanning laboratory is located in the reception area of Wits Mining Institute (WMI) on the basement floor of chambers of mining building, the plan as shown in Figure 3. This space also serves as the kitchen and dining area for the institute with two major entrances. The space has an irregular shape with the dimension of 14.2m × 8.2m × 4.4m. This makes it difficult for the field of view due to the asymmetric pattern of the space from some scan positions. This requires proper planning and measurement that enable visibility of all the targets.

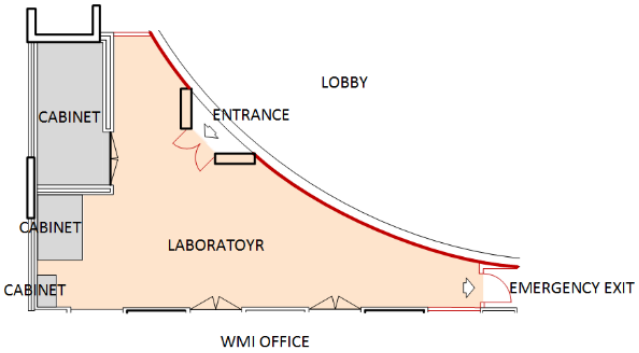

Figure 3 Plan view of the laboratory

The distance from the floor to the roof is measured to be approximately 5m. The space walls are combinations of steel and concrete walls with smooth surfaces, as displayed in Figure 4. The accuracy of the range measurement depends on the scanned surface and the conditions of the experiment environment. The texture of the walls was checked before placing the target. The concrete walls are planar while the steel wall is cylindrical in shape.

The thermal property of the steel wall needs to be considered during the scanning of the laboratory because the steel wall is prone to expansion and contraction when there is a change in temperature. This will also affect the reflectivity of the surface. The temperature fluctuations occur especially during the daytime when the temperature

goes higher and become lower in the evening. Therefore, the surrounding temperatures need to be taken into account during scanning in order to restrain the impact of the thermal movement of the steel wall.

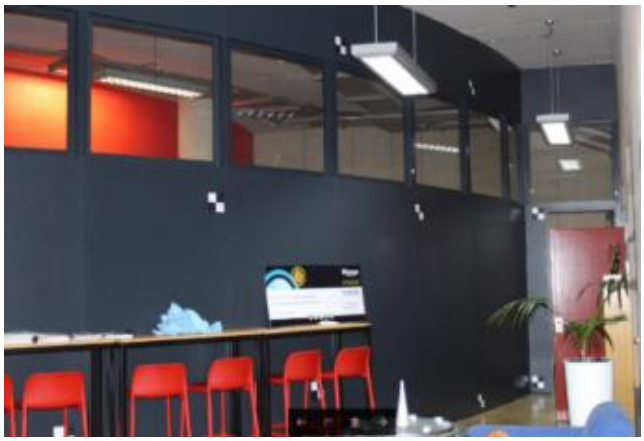

(a) The steel wall

(b) The concrete wall

Figure 4 The space walls of the laboratory

The scanning laboratory was set up with total number of 40 Trimble checkboard targets (in Figure 5), with 34 targets placed on the walls and 5 targets on the roof. The length of the space was approximately 15m. At this observable distance, the scanner can acquire point cloud at high scanning speed and wide field of view that can rotate in both the vertical and horizontal range through 360-degree view. With this short-range space, there will be higher accuracy, as the distance becomes longer the lesser the accuracy of the scan produced (Feng 2012). The positioning of the beacon is important in order to ensure full visibility of all the targets from the control beacon (seeing in Figure 6). These range and angular observations depend on the set up of this beacon to prevent poor visibility and obstructions of the scan. It is obvious that the position of the scanner has an influence on the angle of incidence. The larger the incidence the lower the density of the resulting point clouds. Also, the increase in incidence angle leads to reduction in the intensity of the reflected beam. All these factors were considered in the positioning of the control beacon.

Figure 5 An example of Trimble checkboard target

Figure 6 The control beacon bolted on the floor

3.2 Control beacon design

In ensuring accurate and high precision scans, 1.2m height control beacon with 5/8 inches thread was set up for the positioning of the scanners. The use of the beacon will add value to the quality of the scans by preventing error that may occur due to the movement of the tripod and tribrach. This 5/8 inches thread is a standard dimension that works perfectly with all kinds of surveying instruments. The control beacon was bolted to the floor to ensure its stability. After considering the geometry of the space, the position of the beacon was selected to allow all the targets to be seen during scanning. Photos of this beacon will be displayed at the later stage in the paper.

The materials used for the construction of the beacon are sand, stone, cement, anchor rod, forced-centring plate, and thick plastic pipe. The concrete mix proportions for the construction of the beacon depends on required uniaxial compressive strength level of the resulting beacon. The cure period for the construction of the beacon should be at least 28 days.

3.3 Target design and placement

Trimble laser scanning checkboard target was used for the scanning laboratory. This lightweight 3D imaging target have adhesive material for easier placement on a smooth surface without drilling holes or using any additional messy adhesive. This selected target was made of four alternating black and white squares with edges touching one another at the centre. The dimension of the target was designed based on the distance between the scanner and the control targets. At maximum range of 15m it is possible to view all the targets, 15cm × 15cm dimension of the target will be a good design for the scanning laboratory. The targets were systematically placed on the walls and the roof thereby ensuring visibility from the control beacon. A total number of 40 targets were used, with 11 targets on the steel wall, 23 on the concrete wall and the other 5 targets were placed on the roof. All the targets were placed for sufficient coverage and angular readings, so as to avoid incidence where the scanner could not see all the targets. These targets were named according to the placement in the room. Targets were placed at various elevations and distributed spatially as evenly as possible in order to obtain a spatially uniform registration error. Presence of shiny materials such as metals or mirror surfaces are avoided in the laboratory due to the specular reflective nature. Materials of this nature reflect few or no signal back to the laser scanner.

4 Surveying Control

The survey of the traversing and levelling took a few stages which are discussed in detail below.

4.1 Survey of the control beacon

We did the survey work during stable environment in order to limit the problems associated with high traffic and high level of student activity. The sketch Figure 7(c) shows the closed traversing method. The coordinates of the control points are displayed in Table 1.

4.2 Survey of the targets

In order to get the targets coordinates, besides the Control Beacon and control points T002 and T003, an additional

(a) Images of survey

(b) Images of survey

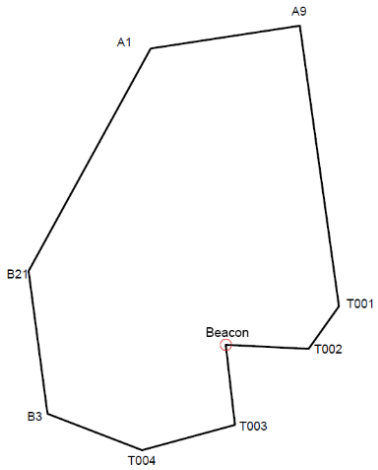

(c) The closed traverse route

Figure 7 Survey of the control beacon

Table 1 The coordinates of the control points

Point	Coordinate		
	Y (m)	X (m)	Z (m)
A1	97282.276	2898380.165	1758.7350
A9	97262.063	2898377.089	1759.2363
T001	97256.788	2898414.891	1760.8756
T002	97260.880	2898420.645	1760.8829
Beacon	97272.103	2898420.075	1762.0062
T003	97270.861	2898430.888	1760.8805
T004	97283.443	2898434.292	1760.8838
B3	97296.235	2898429.386	1761.6711
B21	97298.807	2898410.153	1760.4144

two temporary setups were added throughout the available space in the scanning part with the idea in mind of good network geometry, namely strong angles between the setups that are between 45 and 90 degrees and avoiding small

angles or larger angles close to 180 degrees, between the setups. The positions of the temporary setups were also chosen to allow the maximum number of targets to be seen at each setup, ensuring covering all targets.

The targets coordinates are obtained from the distance and angular measurements based on the knowledge of the location of the Control Beacon and three temporary setups. The surveying coordinates of all targets are displayed in Table 2.

Table 2 Coordinates of targets

Number	Y (m)	X (m)	Z (m)
R1	97270.909	2898426.826	1765.157
R2	97269.975	2898423.717	1765.163
R3	97271.510	2898422.380	1765.168
R4	97271.625	2898418.915	1765.151
R5	97267.201	2898418.813	1765.155
S2	97264.912	2898418.160	1763.064
S3	97264.951	2898417.839	1761.010
S4	97268.548	2898422.871	1764.736
S5	97269.092	2898424.013	1763.036
S6	97268.540	2898422.854	1761.338
S8	97269.597	2898425.387	1764.559
S9	97269.911	2898426.575	1763.074
S10	97270.131	2898427.891	1764.569
S11	97270.134	2898427.922	1761.022
S12	97270.442	2898429.787	1763.222
S13	97270.373	2898429.780	1761.036
C1	97265.586	2898417.142	1764.191
C2	97267.198	2898417.352	1764.207
C3	97269.603	2898417.662	1764.209
C4	97269.605	2898417.671	1762.607
C5	97269.604	2898417.675	1760.994
C7	97269.800	2898416.984	1762.600
C8	97269.801	2898417.005	1760.991
C9	97269.945	2898415.806	1764.194
C10	97270.930	2898415.615	1764.188
C11	97272.909	2898415.880	1763.790
C12	97273.055	2898418.425	1764.185
C13	97273.011	2898418.751	1761.183
C14	97272.781	2898420.425	1763.185
C15	97272.353	2898423.562	1764.789
C16	97272.524	2898422.333	1762.989
C17	97272.314	2898423.853	1761.395
C18	97272.030	2898425.914	1764.789
C19	97272.195	2898424.753	1763.587
C20	97271.843	2898427.375	1762.992
C21	97264.976	2898416.975	1763.768
C24	97268.311	2898420.938	1764.917
C25	97268.196	2898421.781	1763.238
C26	97268.294	2898421.123	1760.999

5 The Scanners

The FARO, a static 3D laser scanner and uGPS, a mobile 3D laser scanning system are tested in this research.

5.1 FARO

The FARO® Laser Scanner Focus3D X130, shown in Figure 8, is a high-speed three-dimensional laser scanner for detailed measurement and documentation. The FARO Focus3D X130 uses laser technology to produce exceedingly detailed three-dimensional images of complex environments and geometries in only a few minutes. The resulting images are an assembly of millions of 3D measurement points. This scanner has a maximum range of 130 meters and collects laser observations between 122000 and 976000 points per second. In addition to the laser observations, the scanner is also fitted with a camera able to capture 360-degree imagery. By utilizing the captured imagery, the point cloud can be colorized creating a true 3D colour environment of the captured data. This scanner is able to do a full 360-degree scan in less than 10 minutes depending on the requirements. It is fitted with GPS, Barometer, Compass and Dual Axis Compensator. The performance specification is displayed in Table 3.

Figure 8 FARO® Laser Scanner Focus3D X130

5.2 uGPS Rapid Mapper™

uGPS Rapid Mapper™, shown in Figure 9, generates accurate 3D point cloud data from a mobile platform, allowing for large areas to be scanned very rapidly. This functionality creates opportunities for a wide range of mining applications, such as mine planning, shaft/raise inspection, geotechnical control and ventilation monitoring. The performance specification is displayed in Table 4.

The uGPS Rapid Mapper™ is a cutting-edge scanning tool with 3D tunnel mapping capabilities- all in a small, portable and versatile package. With its unmatched mobile

capabilities and ease of use straight out of the box, this technology is a welcome solution for the modern underground mines of today.

uGPS Rapid Mapper™ offers unprecedented performance due to its construction, which includes 2 laser scanners, an inertial sensor, an on-board computer, optional Wi-Fi connectivity, and an RFID tag reader. This widens your potential uses to incorporate open loop scanning, closed loop scanning, and even vertical scanning, too.

Table 3 Performance specification of FARO® Laser Scanner Focus3D X130

Range	0.6-130m
Measurement speed	up to 976,000 points/second
Ranging error2	±2mm
Ranging noise	@10m – raw data: 0.3mm @90% refl. @25m – raw data: 0.3mm @90% refl. @25m – raw data: 0.3mm @91% refl. @25m – raw data: 0.3mm @92% refl.
Integr. colour camera	Up to 70 mio. Pixel
Laser class	Laser class 1
Weight	5.2kg
Multi-Sensor	GPS, Compass, Height Sensor, Dual Axis Compensator
Size	240 × 200 × 100mm
Scanner control	via touchscreen display and WLAN

Figure 9 uGPS Rapid Mapper™

Table 4 Performance specification of uGPS Rapid Mapper™

Maximum range	20 m
Data acquisition rate	10,820 points per second
Scanner line speed	20 Hz
Resolution	0.5° in cross-section
Field of view	270°
Laser safety class	Class 1 (eye safe)
Accuracy (open-loop)	0.5% of distance travelled
Accuracy (closed-loop)	< 0.05 m at control points
Weight	12 kg
Size	200 × 300 × 300mm

6 Experiment and Data Analysis

6.1 Data acquisition

6.1.1 Master scanning

The FARO® Laser Scanner Focus3D X 130 was used to acquire master point clouds of the laboratory, supported by Eugene Pretorius and Associates (EPA) Ltd. 5 different scans were necessary to achieve a complete 3D reconstruction of the scene. The master point cloud was registered based on 39 targets (the coordinates can be seen in Table 2) which were coordinated with Trimble total station as described in Section 4. The final registration error was about 1 cm, which contains the point clouds stitching error and artificial point selection error. The master point cloud contains more than 27 million points, visualized in Cloud Compare (http://www.cloudcompare.org/) and shown in Figure 10.

Figure 10 Point cloud of laboratory acquired by FARO.

6.1.2 MLS scanning

The uGPS Rapid Mapper™ was used to MLS point cloud mounted on a trolley (in Figure 11). The moving speed is about 1 km/h. We employed both open route and closed route to acquire two point clouds under different accuracy for the laboratory, supported by RAMJACK Technology Solutions.

The MLS point cloud contains more than 27 million points, visualized in Cloud Compare and shown in Figure 12.

Figure 11 MLS using uGPS Rapid Mapper™

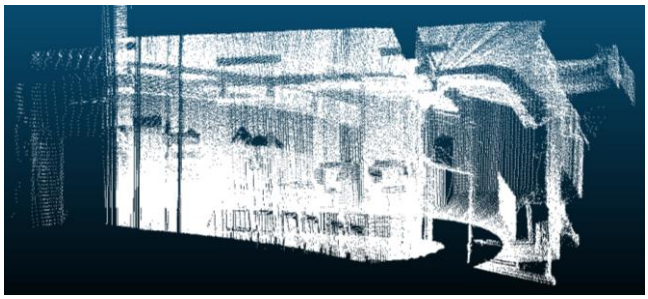

Figure 12 Point cloud of laboratory acquired by uGPS at open route

6.2 Software and process

6.2.1 Software

The accuracy testing experiment of the master point cloud and the MLS point cloud is completed in Cloud Compare (http://www.danielgm.net/cc/), a 3D point cloud editing and processing software. Originally, Cloud Compare has been designed to perform direct comparison between dense 3D point clouds. It relies on a specific octree structure that enables great performances when performing this kind of task. Moreover, as most point clouds were acquired by terrestrial laser scanners, Cloud Compare was meant to deal with huge point clouds on a standard laptop-typically more than 10 million points. Soon after, comparison between a point cloud and a triangular mesh has been supported. Afterwards, many other point cloud processing algorithms (such as registration, resampling, statistics computation, etc.) have followed as well as display enhancement tools (custom colour ramps, colour & normal vectors handling, calibrated pictures handling, OpenGL shaders, plugins, etc.). Moreover, the M3C2 plugin, which is a unique way to compute signed and robust distances directly between two point clouds, is available to compare two clouds directly for users these years. Taking into account its advantages, this study chose Cloud Compare for point cloud processing.

6.2.2 Process

Because of the points obtained by MLS are uncoloured and sparse, the targets can't be verified in the cloud. Therefore, we compared the M3C2 distance between MLS cloud and master cloud.

The MLS point cloud from uGPS Rapid Mapper™ is aligned to the cleaned master point cloud by means of the iterative closest point (ICP) registration method implemented in Cloud Compare. Then Point clouds of furniture and other movable objects are manually deleted in both master point cloud and MLS point cloud to avoid the experimental error caused by object movement (James et al 2017). The aligned point cloud is shown in Figure 13.

Figure 13 The aligned point cloud. The color points are from FARO and the white points are from uGPS

The signed distance between the MLS point cloud and master point clouds are then computed, using the Cloud Compare M3C2 plugin, which implements the Multiscale Model to Model Cloud Comparison method. It allows a direct comparison of 3D points, without the need of a preliminary meshing or gridding phase. For M3C2 process, cloud #1 is uGPS cloud, cloud #2 is FARO cloud. We use the 'Guess params' function to get appropriate parameters for M3C2 distance calculating, and the core point is cloud #1. The normal scale is set to 0.028732, projection scale is set to 0.028732, max depth is set to 0.877179, and the registration error is set to 0. The M3C2 cloud is shown in Figure 14. The histogram of the M3C2 distance is shown in Figure 15.

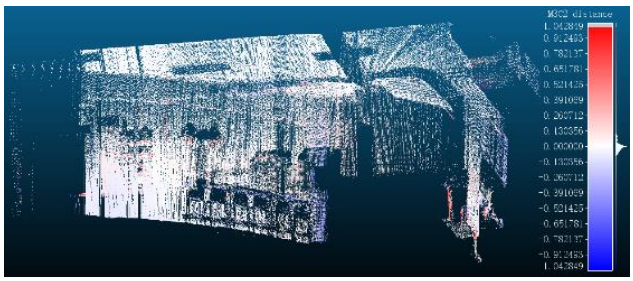

Figure 14 M3C2 cloud. The grey points are the points without any corresponding points in the MLS cloud

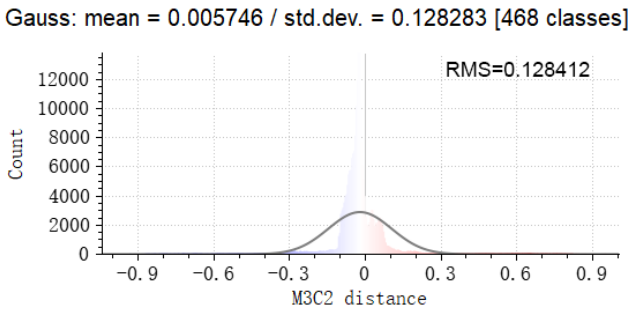

Figure 15 Histogram of the M3C2 distance (m).

6.3 Data analysis

6.3.1 Master point cloud

The targets' centre in the master cloud are localizing and the coordinates are compared with true value (surveying coordinates). The differences are displayed in Table 5. As we can see, the maximum σ is 2.38 cm. The standard deviation of σ is equal to 1.08 cm that means the master point cloud is of a relatively high accuracy.

Table 5 Differences between the targets' coordinate from master cloud and survey

Number	DY (m)	DX (m)	DZ (m)	σ (m)
R1	-0.001	-0.022	-0.009	0.0238
R2	0.006	-0.014	-0.004	0.0157
R3	-0.004	0.000	0.006	0.0077
R4	0.001	0.003	-0.008	0.0086
R5	0.005	-0.005	-0.006	0.0093
S2	-0.007	-0.008	0.000	0.0106
S3	-0.005	-0.001	0.001	0.0052
S4	-0.001	-0.005	0.003	0.0059
S5	0.001	-0.007	0.004	0.0079
S6	0.001	0.001	0.006	0.0058
S8	0.002	0.002	0.005	0.0058
S9	0.001	-0.008	0.001	0.0085
S10	-0.001	-0.006	-0.004	0.0073
S11	0.006	-0.016	-0.005	0.0182
S12	0.002	-0.007	-0.002	0.0075
S13	0.002	-0.010	-0.003	0.0106
C1	0.003	-0.004	-0.001	0.0051
C2	-0.002	-0.004	0.002	0.0049
C3	-0.007	-0.009	0.003	0.0118
C4	-0.004	-0.008	0.002	0.0092
C5	0.001	-0.004	0.006	0.0073
C7	-0.008	-0.011	-0.003	0.0145
C8	-0.009	-0.009	-0.004	0.0133
C9	-0.008	-0.005	-0.002	0.0101
C10	-0.008	-0.010	-0.004	0.0136
C11	-0.006	-0.014	0.001	0.0153
C12	-0.002	-0.012	-0.001	0.0122
C13	-0.011	0.008	0.000	0.0136
C14	-0.004	-0.005	-0.001	0.0068
C15	-0.004	-0.008	-0.002	0.0089
C16	-0.002	-0.007	-0.003	0.0079
C17	-0.006	-0.005	0.002	0.0081
C18	-0.004	-0.006	-0.009	0.0115
C19	0.005	-0.010	0.003	0.0114
C20	0.006	-0.002	-0.001	0.0065
C21	-0.006	-0.009	0.002	0.0110
C24	-0.010	-0.007	0.003	0.0126
C25	-0.005	-0.006	0.003	0.0084
C26	0.002	-0.010	0.003	0.0106

Note: $\sigma = \sqrt{DY^2 + DX^2 + DZ^2}$

6.3.2 MLS point cloud

As shown in Figure 15, the histogram of the M3C2 distance tends to normally distributed. The mean of 0.57 cm proves that there is no significant offset between the point clouds. It means that we have done an excellent alignment between MLS cloud and master cloud. While the standard deviation of 12.83 cm and the RMS of 12.84 cm mean the noise is relatively significant, which expose relatively low accuracy of the uGPS scanning without control point.

7 Conclusion and Recommendation

Since laser scanning systems become more and more popular in mining, we set a laboratory for TLS systems' accuracy and precision testing. Forty high quality and reliable targets were attached to the walls and ceiling to evaluate the accuracy of FARO® Laser Scanner Focus3D X130. Comparing the difference between the coordinates in FARO point cloud and of surveying, the accuracy of FARO is almost 1 cm in our experiment. It shown FARO is at relatively high accuracy level. The uGPS Rapid Mapper™ got the laboratory point cloud much fast than FARO. However, it is not suitable for mining surveying because the accuracy of the uGPS scanning without control point is relatively low.

References

Barber, D., J. Mills and S. Smith-Voysey, 2008. Geometric validation of a ground-based mobile laser scanning system. Isprs Journal of Photogrammetry & Remote Sensing, **63**(**1**): 128 - 141.

Botes, D., 2013. Accuracy assessment: Mobile laser scanning versus competing methods. The South African Surveying and Geomatics Indaba (SASGI) Proceedings, Ekurhuleni, South Africa, July 23 - 24, 2013.

Feng, Q., 2012. Practical application of 3D laser scanning techniques to underground projects. ISRM-Swedish national task A survey of 3d laser scanning techniques for application to rock mechanic. BeFo Report, **114**, 67.

Grehl, S., M. Donner, M. Ferber, A. Dietze, H. Mischo and B. Jung, 2015. Mining-rox-mobile robots in underground mining. International Future Mining Conference, Sydney, NSW, November 4 - 6, 2015

Jafari, B., A. Khaloo and D. Lattanzi, 2017. Deformation tracking in 3D point clouds via statistical sampling of direct cloud-to-cloud distances. Journal of Nondestructive Evaluation, **36**(**4**): 65.

James, M.R., S. Robson and M.W. Smith, 2017. 3-D uncertainty-based topographic change detection with structure-from-motion photogrammetry: precision maps for ground control and directly georeferenced surveys. Earth Surface Processes & Landforms, **42(12)**: 1769 - 1788.

Kaartinen, H., J. Hyyppä, A. Kukko, A. Jaakkola and H. Hyyppä, 2012. Benchmarking the performance of mobile laser scanning systems using a permanent test field. Sensors, **12**(**9**): 12814 - 12835.

Lindenbergh, R. and P. Pietrzyk, 2015. Change detection and deformation analysis using static and mobile laser scanning. Applied Geomatics, **7**(**2**): 65 - 74.

Mao, Q., L. Zhang, Q. Li, Q. Hu, J. Yu, S. Feng, W. Ochieng and H. Gong, 2015. A least squares collocation method for accuracy improvement of mobile LiDAR systems. Remote Sensing, **7**(**6**): 7402 - 7424.

Mukupa, W., G. W. Roberts, C. M. Hancock and K. Al-Manasir, 2016. A review of the use of terrestrial laser scanning application for change detection and deformation monitoring of structures. Empire Survey Review, **49**(**353**): 99 - 116.

Puente, I., H. González-Jorge, J. Martínez and P. Arias, 2013. Review of mobile mapping and surveying technologies. Measurement Journal of the International Measurement Confederation, **46**(**7**): 2127 - 2145.

Vaaja, M., J. Hyyppä, A. Kukko, H. Kaartinen, H. Hyyppä and P. Alho, 2011. Mapping topography changes and elevation accuracies using a mobile laser scanner. Remote Sensing, **3**(**12**): 587 - 600.

Williams, K., M. J. Olsen, G. V. Roe and C. Glennie, 2013. Synthesis of transportation applications of mobile LIDAR. Remote Sensing, **5**(**9**): 4652 - 4692.

Zlot, R. and M. Bosse, 2014a. Three-dimensional mobile mapping of caves. Journal of Cave & Karst Studies the National Speleological Society Bulletin, **76**(**3**): 191 - 206

Zlot, R. and M. Bosse, 2014b. Efficient large-scale three-dimensional mobile mapping for underground mines. Journal of Field Robotics, **31**(**5**): 731 - 752.

.